Classification of arterial and venous cerebral vasculature based on wavelet post-processing of CT perfusion data

Lukas Havla[1†], Moritz J. Schneider[1†], Kolja M. Thierfelder[2], Sebastian E. Beyer[2], Birgit Ertl-Wagner[2], Maximilian F. Reiser[2], Wieland H. Sommer[2], and Olaf Dietrich[1]

[1] Josef Lissner Laboratory for Biomedical Imaging, Institute for Clinical Radiology, Ludwig-Maximilians-University Hospital Munich, Marchioninistr. 15, 81377 Munich, Germany

[2] Institute for Clinical Radiology, Ludwig-Maximilians-University Hospital Munich, Marchioninistr. 15, 81377 Munich, Germany

† Lukas Havla and Moritz J. Schneider contributed equally to this work.

ELECTRONIC PREPRINT VERSION:
This is the peer reviewed version of the following article: Med Phys 2016; **43**(2): 702–709, which has been published in final form at <URL:http://dx.doi.org/10.1118/1.4939224>.

Abstract

Purpose: **The purpose of this study was to propose and evaluate a new wavelet-based technique for classification of arterial and venous vessels using time-resolved cerebral CT perfusion data sets.**

Methods: **14 consecutive patients (mean age 73 years, range 17-97) with suspected stroke but no pathology in follow-up MRI were included. A CT perfusion scan with 32 dynamic phases was performed during intravenous bolus contrast-agent application. After rigid-body motion correction, a Paul wavelet (order 1) was used to calculate voxelwise the wavelet power spectrum (WPS) of each attenuation-time course. The angiographic intensity *A* was defined as the maximum of the WPS, located at the coordinates *T* (time axis) and *W* (scale/width axis) within the WPS. Using these three parameters (*A, T, W*) separately as well as combined by (1) Fisher's linear discriminant analysis (FLDA), (2) logistic regression analysis (LogR), or (3) support-vector-machine analysis (SVM), their potential to classify 18 different arterial and venous vessel segments per subject was evaluated.**

Results: **The best vessel classification was obtained using all three parameters *A&T&W* (area under the curve (AUC): 0.953 with FLDA and 0.957 with LogR or SVM). In direct comparison, the wavelet-derived parameters provided performance at least equal to conventional attenuation-time-course parameters. The maximum AUC obtained from the proposed wavelet parameters was slightly (although not statistically significantly) higher than the maximum AUC (0.945) obtained from the conventional parameters.**

Conclusions: **A new method to classify arterial and venous cerebral vessels with high statistical accuracy was introduced based on the time-domain wavelet transform of dynamic CT perfusion data in combination with linear or non-linear multidimensional classification techniques.**

Keywords:

Diagnostic imaging; Angiography; Discriminant analysis; Cerebrovascular stroke; Perfusion CT; Wavelet transform

Corresponding author:

Lukas Havla
Josef Lissner Laboratory for Biomedical Imaging,
Institute for Clinical Radiology,
Ludwig-Maximilians-University Hospital Munich,
Marchioninistr. 15, Munich 81377, Germany
E-mail: lukas.havla@med.uni-muenchen.de

Introduction

The retrospective differentiation of concomitantly enhanced arterial and venous vessels in 3D angiographic data sets is an important problem, for which several post-processing approaches have been suggested. This problem arises regularly, e. g., in 3D angiographic data derived from 4D dynamic contrast-enhanced CT perfusion (CTP) data sets, i. e. from multiple (time-resolved) acquisitions of CT data during the passage of a contrast agent bolus through the parenchyma, which provides additional dynamic information for each vessel. Beier et al. [1] demonstrated the potential of post-processing CTP data using temporal maximum intensity projections (tMIP) for depicting (concomitant) arterial and venous enhancement within a single image. An improved approach for the calculation of angiographic datasets from CTP data was proposed by Smit et al., who combined temporal filtering the tMIP post-processing [2]. Recently, a new post-processing technique for CTP data based on the time-domain wavelet transform of each voxel time course was shown to provide angiographic images with significantly improved contrast-to-noise ratio and image quality [3].

In general, reducing the dimensionality of the time-resolved 4D CT perfusion data using tMIP or wavelet post-processing impedes the differentiation between arteries and veins. To mitigate this difficulty, several vessel classification strategies based on circulatory features of the dynamic CTP datasets have been employed. Three already clinically evaluated markers are the time of arrival [4], full width at half maximum (FWHM) [5], and the time to peak (TTP) [6]. As recently demonstrated, linear combinations of these circulatory parameters can significantly improve the classification performance compared to each single parameter [7]. Another approach going beyond single-marker mapping was proposed by Thierfelder et al. [8] who implemented a convolution-based multi-parametric fitting algorithm to display the temporal information in a range of colors.

The purpose of this study was to implement and evaluate a new wavelet-based post-processing approach for time-resolved cerebral CT perfusion data sets, which we hypothesize to provide new parameters for the differentiation between arterial and venous vessels. The classification performance of these newly proposed parameters was compared to the performance of conventional markers derived directly from the time-density curves. The calculation of these new parameters relies on the same time-domain wavelet-transform technique that was recently proposed for reconstructing angiographic images [3].

Material and Methods

Wavelet transform

Wavelet transforms are widely used in signal and image processing (e. g. for noise reduction [9]). For analyzing non-periodic and finite data, wavelets are generally better suited than the Fourier transform [10]. While the latter uses trigonometric functions (sin, cos) as basis functions, almost every (typically complex-valued) function whose mean is zero and whose Fourier spectrum features a band-pass like shape can be selected as mother wavelet $\Psi_0(\eta)$ of the wavelet transform.

The continuous wavelet transform $\tilde{f}(t,s)$ of a scalar function $f(\eta)$ (η: dimensionless time parameter) is basically the convolution of the original signal $f(\eta)$ with a function $\Psi_{t,s}(\eta)$ derived from the mother wavelet:

$$\Psi_{t,s}(\eta) = |s|^{(-1/2)}\,\Psi_0\left(\frac{\eta - t}{s}\right)$$

$$\tilde{f}(t,s) = \int f(\eta)\overline{\Psi}_{t,s}(\eta)\,d\eta$$

$$\text{with} \quad \overline{\Psi}_{t,s} := \text{complexcon} \quad \text{jugateof} \quad \Psi_{t,s}$$

The transform parameter *t* is shifting the mother wavelet along the time axis and *s* is the dilation factor of the wavelet. In the discrete case, $\tilde{f}(t,s)$ of $f(\eta)$ is a 2D $M \times N$ (in this study: $M = 32$ *time points,* $N = 128$ scaling factors) matrix, whose squared norm $\left|\tilde{f}_{t,s}(x,y,z)\right|^2$ yields the *wavelet power spectrum* (WPS).

Wavelet-based vessel features

When the wavelet transform is applied (voxelwise) to the time-density curves of CT perfusion data, the resulting WPS describes quantitatively the similarity of the shape of the time-density curve

and the shifted (parameter *t*) and scaled (*s*) mother wavelet. A sparse representation (by a low number of wavelet coefficients that are not close to zero) requires a sufficient similarity between the shape of the mother wavelet and a typical time-density curve of the application under consideration. For CT perfusion data, the time-density curves in the vasculature are characterized predominantly by a single signal lobe representing the first passage of the contrast agent. Consequently, we chose the Paul wavelet [11] of order $m = 1$ for this study, which has a similar shape and is defined as (Figure 1):

$$\Psi_0(\eta) = \frac{2^m i^m m!}{\sqrt{\pi(2m)!}}(1 - i\eta)^{-(m+1)}.$$

The position (t_{peak}, s_{peak}) of the maximum of the WPS describes the required translation (*t*) and scaling (*s*) of the mother wavelet to optimally match the shape of the time-density curve. Thus, t_{peak}, can be interpreted as the bolus delay and s_{peak} as the bolus width in analogy to the conventional time-density-curve parameters TTP and FWHM (Figure 2). A third parameter directly encoded in the WPS peak, is the height (or intensity) *I* of the peak, which can be interpreted as a quantitative measure of (a) the similarity between curve and wavelet shape and (b) the height (i. e., magnitude scaling) of the original time-density curve. The latter property has been previously exploited when *I* was used as angiographic intensity for the presentation of 3D angiographies [3]. Summarized, three parameters (t_{peak}, s_{peak}, *I*) are derived from the WPS peak, which can be used to characterize the contrast-agent flow through a voxel; therefore, we hypothesize that these parameters can be used as new classification features for the differentiation between arterial and venous vessels:

Peak position:

$$(t_{peak}, s_{peak})(x, y, z) = \arg\max_{t,s}\left(\left|\tilde{f}_{t,s}(x, y, z)\right|^2\right)$$

Peak height:

$$I(x, y, z) = \max_{t,s}\left(\left|\tilde{f}_{t,s}(x, y, z)\right|^2\right)$$

To assess the classification performance of these new wavelet-based features in comparison to conventional time-density curve characteristics, a patient study in 14 patients was performed as described below. The conventional characteristics used as standard of reference were: 1) signal maximum MAX, 2) signal TTP, and 3) signal FWHM (cf. Figure 2). As described in detail by Havla et al. [7], the three reference parameters were derived voxelwise from the time-density curves by fitting a gamma-variate function to the measured data.

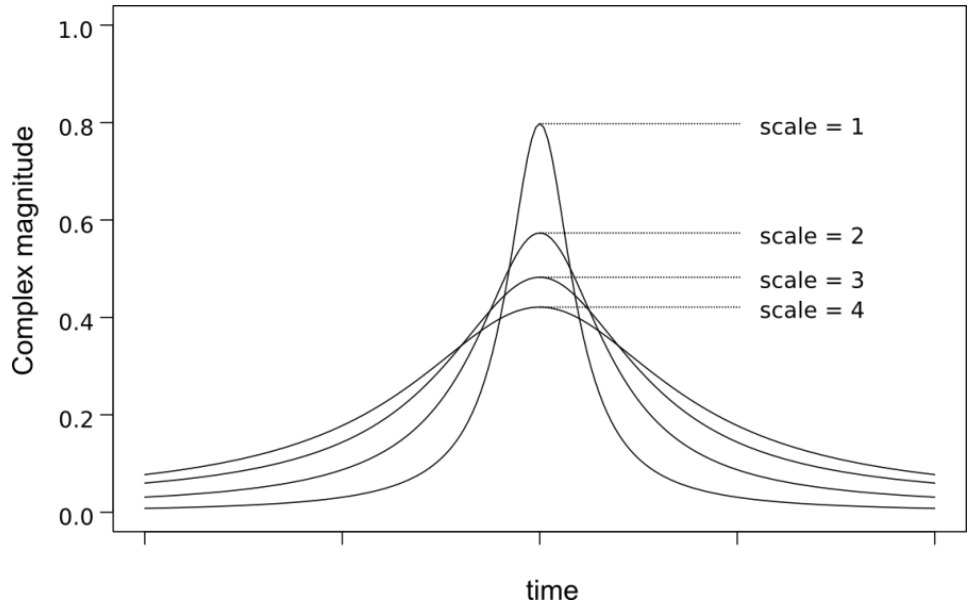

Figure 1. The magnitude of the (complex) Paul wavelet function is shown at four different scale steps. This visualization illustrates the visual similarity between the wavelet function and the CT time-density curves to be analyzed (cf. Fig. 2 (A) and (C)).

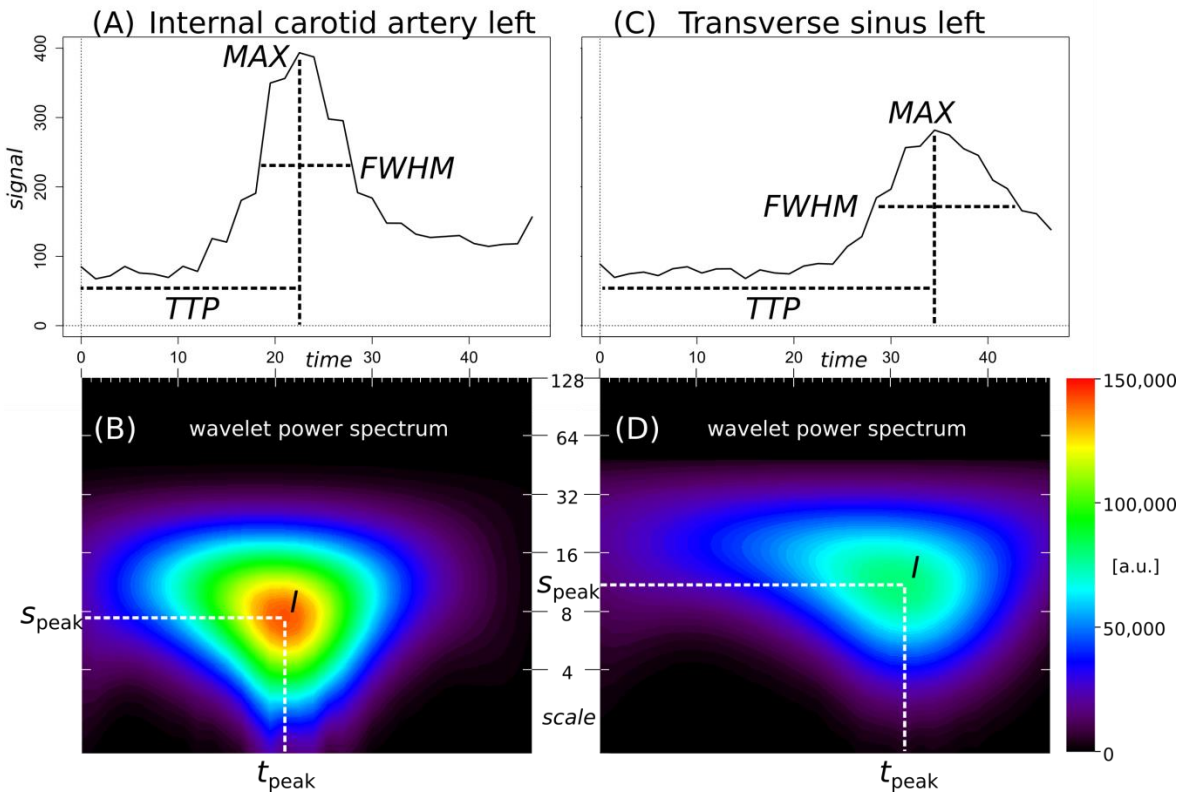

Figure 2. Two sampled time-density curves from an arterial (A) and a venous vessel (C) of a 76 y/o male patient and their corresponding wavelet power spectra below (WPS). The three wavelet parameters (I, t_{peak}, s_{peak}) are shown in the WPS maps (bottom row B, D).

Patient study and data acquisition

The institutional review board waived informed consent for this retrospective study. Inclusion criteria were the availability of 4D perfusion data of patients with suspected stroke and without pathology on follow-up MRI. Fifteen consecutive patients who had been examined between December 22nd, 2012 and February 1st, 2013 met the inclusion criteria. From this cohort we excluded one patient without standardized contrast agent application. In the final patient group ($N = 14$, mean age 73 years, range 17-97) were six females. The same patient population was already evaluated in a recent study by Havla et al. [7]; the methods and results of this earlier study were used as standard of reference for the present evaluation as described below.

For data acquisition, a dual-source CT system (SOMATOM Definition Flash, Siemens Healthcare, Forchheim, Germany) was used in single-source mode. The temporal resolution of 1.5 s resulted in an acquisition time of 48 s (32 sweeps in table shuttle mode). The scanned 3D volume spanned over 99 mm in the z-axis; 99 thin (1.0 mm increment and 1.5 mm slice thickness) slices were reconstructed. Tube voltage and tube current were set to 80 kV and 200 mAs, respectively. 35 mL of iomeprol-350 (Imeron 350, Bracco Imaging Deutschland, Konstanz, Germany) were injected at a flow rate of 4.5 mL/s prior to a saline flush of 40 mL.

Post-processing

For all post-processing tasks, a personal computer equipped with 16 GB RAM and a conventional Intel i5 processor was used. Unless indicated otherwise, all computational steps were conducted with an in-house developed software (PMI, Platform for Medical Imaging v0.4 [12]).

Motion correction and parameter maps

As a first step, the open source elastix toolbox [13] was used to perform rigid-body motion correction. Afterwards, 32 × 99 × 15 (phases × slices × patients) CT images were re-imported into PMI. The three quantitative wavelet parameters (I, t_{peak}, s_{peak}) as well as the conventional parameters (MAX, TTP, FWHM) described above were then calculated for each image voxel of the (dynamic) 4D data sets,

resulting in two sets of three 3D parameters maps for each subject.

Vessel definition

To assess the classification performance of the proposed wavelet-based features, 11 arterial and 7 venous vessels were identified by two experienced readers in each subject. For these 18 different vessel segments, regions of interest (ROIs) were defined with a varying number of voxels (29.9±30.0 voxels) adapted to the vessel anatomy (the ROIs could be freely defined and were not restricted to e. g. circular or rectangular shapes): 11 in cerebral arteries (2× internal carotid / 1× basilar / 2× M1 middle cerebral / 2× P1 posterior cerebral / 2× M2 middle cerebral / 2× leptomeningeal collaterals) and 7 in (venous) vessels (1× sagittal / 2× transverse / 2× sigmoid sinus and 2× bridging veins to the sagittal sinus). Vessel walls were excluded to minimize partial volume effects.

The mean value of each ROI applied to each 3D parameter map was taken yielding two sets of three parametric mean values (I, t_{peak}, s_{peak}) and (MAX, TTP, FWHM) for every patient's vessel segments. Intra-individual normalization was then used to compensate for patient-specific hemodynamics: every parameter was divided by its mean value in the two carotid arteries of each patient. The normalized parameters (of both wavelet and conventional analysis) were named as follows [7]:

- A (normalized WPS intensity I or normalized time-density-curve maximum MAX);
- T (normalized peak position t_{peak} along the time axis or normalized TTP);
- W (normalized peak position s_{peak} along the scale ("width") axis or normalized FWHM).

Statistics

All statistical calculations were performed using R (R: A language and environment for statistical computing; version 3.1.0; R Foundation for Statistical Computing, Vienna, Austria).

Fisher's linear discriminant analysis

FLDA is a statistical method to reduce the dimensionality of data. By finding an optimal linear combination of a given feature set, the differentiation between two (or more) classes can be improved compared to using each feature individually [14, 15]. FLDA was applied using either two out of three alternately combined parameters or using all three parameters as input. The used FLDA tools were available as open-source software in R packages (*Bioconductor* [16] and *CMA* [17]).

Support vector machine analysis

Support vector machine (SVM) approaches [18] are used for regression and classification purposes. In contrast to FLDA, classes are not only separated by a (linearly defined) hyperplane, but by a more complex non-linear hypersurface, representing the largest separation between the two classes. The employed radial SVM classifier [19] (referred to as SVMr) uses a radial basis function kernel, allowing for increased flexibility and potentially improved classification compared to the linear FLDA approach but at the cost of higher computational power and more difficult interpretability.

Logistic regression analysis

As a third classifier, logistic regression analysis (LogR) was performed for each feature combination. Logistic regression and SVM training was done using the open-source R package *caret* [20].

ROC curve analysis

The three aforementioned normalized parameters (A, T, W) were evaluated – individually and combined – by receiver operating characteristic (ROC) analyses. The area under the curve (AUC) and the diagnostic accuracy (i. e., 1 – cross-validation error as described below) were determined and used for performance comparisons of the seven different single or combined features. The optimal threshold for separation between arteries and veins was defined as the point maximizing the sum of sensitivity and specificity [21].

The calculation of ROC curves including their statistical measures was performed with the open-source R package pROC [22]. DeLong's test was applied for probing statistical significance between two ROC curves [22, 23].

Since more than one statistical test was conducted within the same data frame, the Bonferroni correction [24] was applied by setting $p = 0.05 / 23 = 0.0021$.

Cross-validation for accuracy estimation

To evaluate the performance of the trained models, we used repeated n-fold cross-validation (as

recommended by Kohavi [25]). The number of folds was set to 9, which simplified data sampling because the total number of samples can be factorized by 3 ($243 = 3^5$), and repetitions were set to 10,000. Accordingly, the models were trained 9-fold in 10,000 iterations using 8 out of 9 subsets and tested against the 9th subset. The error rate C_{error} was determined as the total number of false positives and false negatives per sample size divided by all 90,000 iterations; 1 - C_{error} was calculated as estimation of the accuracy.

Linear correlation
To assess the degree of concordance between different parameters, linear Pearson correlation coefficients were calculated.

Results

Nine of 252 ROIs (18 vessel segments × 14 included patients) were excluded due to either incomplete z-axis coverage of all vessel segments ($n = 3$) or due to severe image registration artifacts in distal slices ($n = 6$). For every included vessel segment, three (*A*, *T*, *W*) parameter mean values were analyzed.

ROC curve analyses

Classifier performance
The AUCs and cross-validation-based accuracies (1 - C_{error}) of all evaluated ROC curves were calculated for each classification approach (FLDA, LogR, and SVMr); the resulting values are summarized in Table 1. For the FLDA, the optimal thresholds for linear discrimination between arteries and veins are also provided.

One-parameter classifiers
The best-performing single-parameter classifier was *T* (with respect to both AUC and cross-validation-based accuracy); with the optimal threshold, the AUC was 0.866 (cross-validation-based accuracy: 77.5 %). W yielded an AUC of 0.821 (accuracy: 77.2 %) and A an AUC of 0.731 (accuracy: 65.4 %).

Two-parameter and three-parameter classifiers
The best combined classifier based on 2 features was the combination of *A* & *T* with AUCs between 0.945 and 0.949 (cross-validation-based accuracies between 84.6 % and 90.5 %). Combining *A* & *W* resulted in AUCs between 0.915 and 0.953 (accuracies between 82.7 % and 88.5 %) and *T* & *W* in AUCs between 0.864 and 0.900 (accuracies between 78.2 % and 79.8 %).

The 3-parameter combination *A* & *T* & *W* yielded the highest AUCs between 0.953 and 0.957 (accuracies between 85.8 % and 90.5 %).

Comparison of classification techniques
Comparing the different classification approaches (Table 1), highest AUCs were obtained by SVMr, followed by LogR and FLDA. In 3 of 4 feature combinations, the SVMr accuracy was the best; only for the combination of T & W, LogR had the best cross-validation-based accuracy.

All ROC curves were tested for significant difference among each other but no p-value was below the Bonferroni-corrected significance level of 0.0021.

Classifier performance evaluation
The 3-parameter vessel classifiers showed better performance (without statistical significance) than the best 2-parameter combination *A* & *T* (DeLong's test, $p = 0.029$) and was significantly better than the best 1-parameter classifier *T* ($p < 0.00001$).

Figure 3 illustrates the threshold functions derived from FLDA ROC analysis. In Figure 4 and Figure 5, the vasculature of two patients is visualized in three different ways. According to Havla et al. [3], the highest coefficient of the wavelet power spectrum was denoted the angiographic intensity information *A*.

Table 1. Results (AUC and estimated accuracy 1 − C_{error}) from statistical ROC curve analysis of FLDA, LogR, and SVMr wavelet classifiers.

	FLDA			LogR		SVMr	
Wavelet features	AUC	1 − C_{error} [%]	Threshold for venous vessels	AUC	1 − C_{error} [%]	AUC	1 − C_{error} [%]
A	0.731	65.4	$A < 0.40$				
T	0.866	77.5	$T > 1.10$				
W	0.821	77.2	$W > 1.04$				
A & T	0.945	84.6	$-0.11 \times A + 0.33 \times T > 0.30$	0.949	86.4	0.949	90.5
A & W	0.915	82.7	$-0.12 \times A + 0.54 \times W > 0.48$	0.931	85.2	0.953	88.5
T & W	0.864	79.3	$0.32 \times T + 0.17 \times W > 0.51$	0.863	79.8	0.900	78.2
A & T & W	0.953	85.8	$-0.11 \times A + 0.26 \times T + 0.15 \times W > 0.38$	0.957	87.7	0.957	90.5

Table 2. Comparison between the wavelet-based and the corresponding reference standard classifiers. For the single parameters, Pearson's correlation coefficient between wavelet and reference parameters is shown.

Classification features	**AUC and DeLong's test**			**Correlation *r***
	Wavelet	Reference	p-value	
A	0.731	0.669	**<0.0001**	0.875
T	0.866	0.871	0.764	0.923
W	0.821	0.789	0.346	0.288
A & T	0.945	0.945	0.943	
A & W	0.915	0.809	**<0.0001**	
T& W	0.864	0.896	0.053	
A & T& W	0.953	0.945	0.349	
	p-values printed in bold are below the significance level of 0.0021			

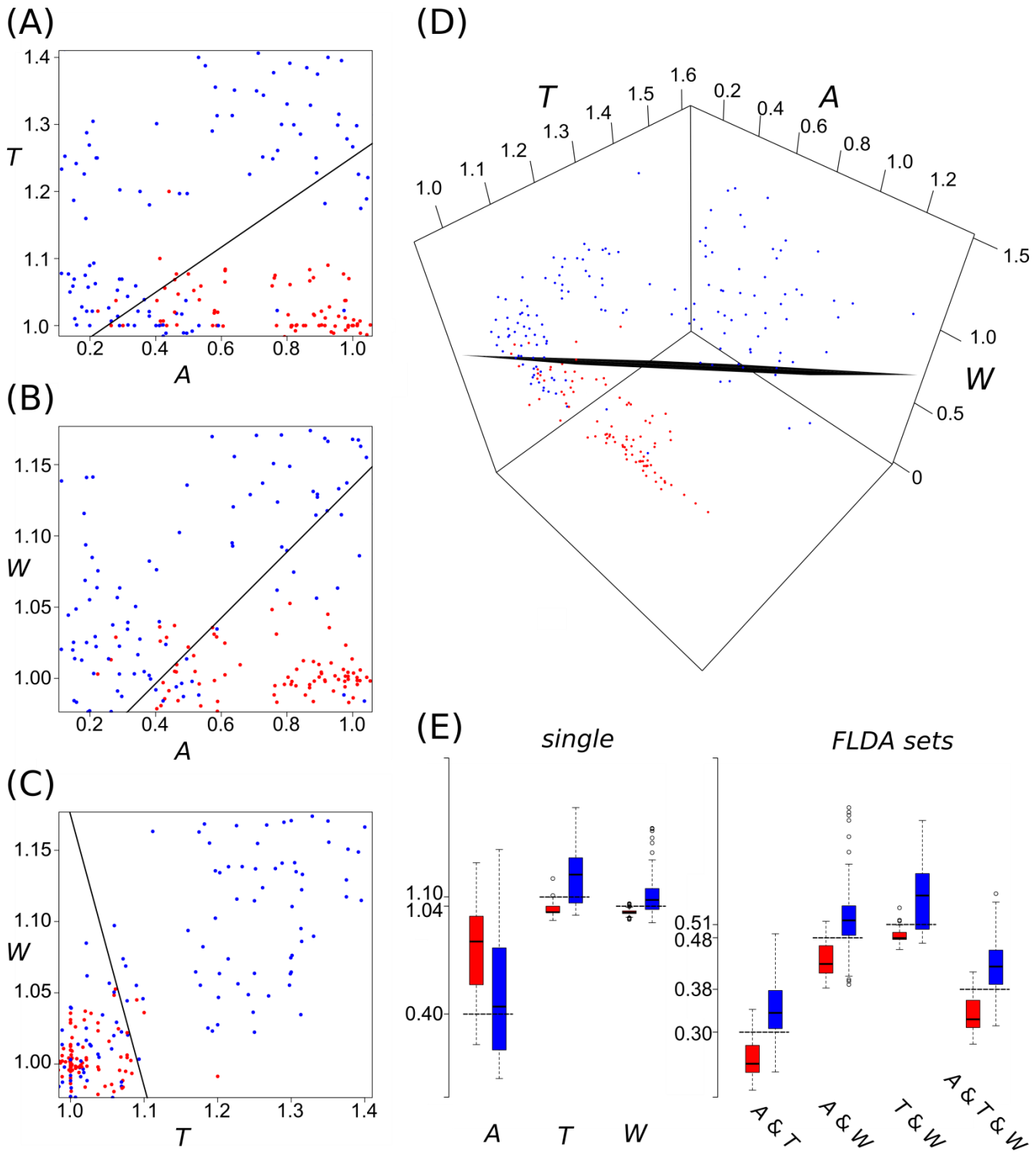

Figure 3. Classification plots of the wavelet parameters. Arterial data are shown in red, venous in blue. The two-parameter FLDA plots are shown in A-C. The solid line represents the optimal threshold as determined by the ROC curve analysis. D contains the 3D plot of the three-parameter FLDA (hyperplane in black). E shows boxplots of all seven calculated parameters (single parameters and parameter combinations; threshold as dashed line); the boxplot of the three-parameter wavelet FLDA combination visualizes very good discrimination between arterial and venous vessels.

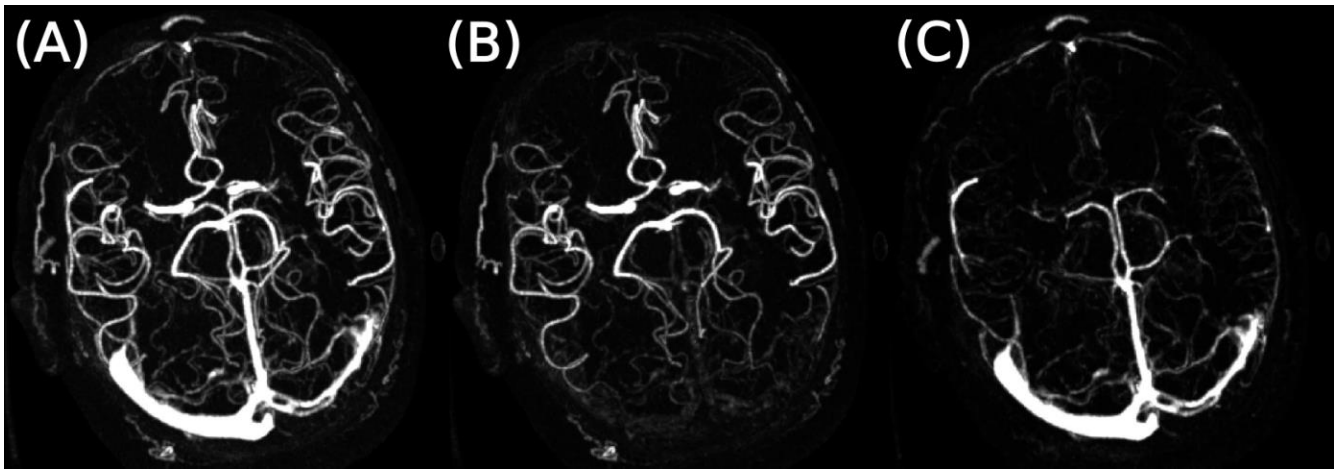

Figure 4. Angiographic images axial view. The left image (A) displays the parameter *A* of the wavelet power spectrum. The other panels use the three parameter FLDA classifier on top of *A* to create a *windowed,* predominantly arterial (B) and venous (C) angiography of a 76 y/o male patient. The *window* level can be changed continuously by the individual reader to increase his/her confidence.

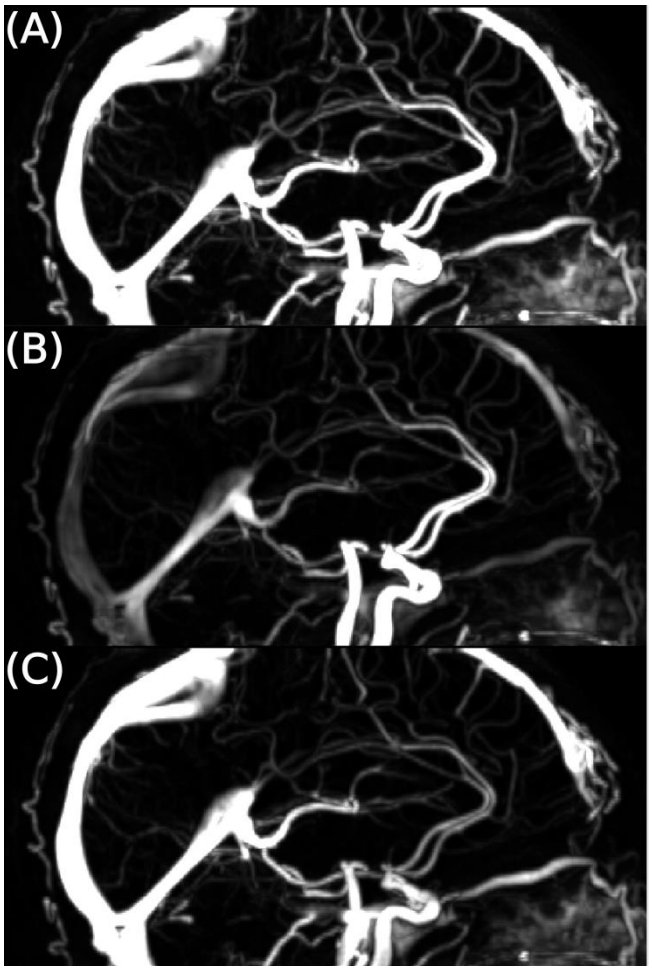

Figure 5. Angiographic images sagittal view. The top image (A) displays the parameter *A* of the wavelet power spectrum. The other panels use the three parameter FLDA classifier on top of *A* to create a *windowed,* predominantly arterial (B) and venous (C) angiography of a 96 y/o female patient.

Linear correlation coefficients

All three wavelet features (*A*, *T*, *W*) were normally distributed according to the Shapiro-Wilk test ($p < 0.00001$). The linear correlation of the parameters *T* and *W* using Pearson's method yielded $r = 0.68$. The correlation coefficients between *A* and *W* as well as *A* and *T* indicated no correlation ($r = 0.06$ and $r = 0.06$).

Comparison to reference standard

DeLong's test showed two significant differences of AUC values between the proposed wavelet-based classification and the conventional time-density-curved derived parameters: 1) for *A* and 2) for *A* & *T* as listed in Table 2. In 4 out of 7 FLDA evaluations, higher AUC values were obtained from the wavelet-based features; in 2 out of 7 evaluations, the conventional features showed higher AUC values. The AUC improvement of the best FLDA classifier (*A* & *T* & *W*) by 0.0075 when using the newly proposed parameters was not statistically significant ($p = 0.349$). Pearson's correlation coefficients are also shown for the pairs of wavelet and reference method parameters (*A, T, W*) in Table 2.

Discussion

Our results show that arterial and venous vessels can be accurately differentiated using the newly proposed wavelet-derived parameters *A* (wavelet power spectrum maximum), *T* (temporal peak position), and *W* (scale-axis peak position). Linear or non-linear combination of more than a single parameter improves vessel classification significantly. The most accurate *single* wavelet-derived parameter was *T* with an AUC of 0.866, followed by *W* and by *A*. The best combination of two parameters was *A* & *T* (AUC: 0.945 with FLDA and 0.949 with LogR and SVMr). Adding the bolus-width-related parameter *W* to the combination of *A* & *T* resulted in a further improvement of the classification performance with a AUCs between 0.953 (FLDA) and 0.957 (LogR, SVMr) corresponding to cross-validation-based accuracies between 85.8 % (FLDA) and 90.5 % (SVMr). This indicates that the statistically weakly related wavelet parameters *A* and *W* as well as *A* and *T* provide complementary vascular information and the parameter-combining classifications exploit their independent information. The validity and robustness of our multi-parameter evaluation was supported by the results of *9*-fold cross-validation.

The multi-dimensional classifiers were trained with three methods (FLDA, LogR, and SVMr) using the complete data set (Table 1). The choice between the different classification approaches FLDA, LogR, and SVMr depends on the objectives of the study. Compared to support vector machines, Fisher's linear discriminant analysis is a relatively simple method. The calculation is straightforward and the visualization of its results is intuitive. There was no significant difference between the classifiers trained with the FLDA and the LogR or SMVr approaches. Although the application of the LogR and SVMr resulted in slightly higher values of the accuracy, the gain in AUC was not statistically significant. Due to the more complex model structure of the non-linear approaches LogR and SVMr as well the minor improvements in classification results, we finally preferred the FLDA for the calculation of arterial and venous angiography data sets.

The panels B and C of Figure 4 are the result of applying the combined wavelet parameter classifiers on angiographic images. Using the information of the three-parameter FLDA classifier, a *windowed* representation – showing predominantly arterial or venous vessels – of the cerebral vasculature can be displayed. Future studies are required to find out if the presented approach may overcome the problem of venous superimposition which hampers the detection of small arterial occlusions especially in timing-invariant CT angiographies [2]. Other conditions in which an isolated representation of arterial vessels might be useful are intracranial stenoses and dissections. On the other hand, the exclusion of a cerebral venous thrombosis requires an isolated representation of venous vessels. Further possible applications of vessel differentiation are conditions like arteriovenous malformations or vasospasm.

A fundamental advantage of the proposed wavelet-based approach is that by using only one methodology (i. e., the time-domain wavelet transform) two so far unrelated tasks in diagnostic imaging and data visualization can be accomplished within one post-processing step: 1) the calculation of high-quality angiographic images and 2) an accurate classification of arterial and venous vessels. Previously proposed methods for vessel classification required the direct measurement of the time to peak or the bolus width, which is substantially impeded by random signal fluctuations (image noise) despite recent advances in the field of noise reduction methods for CT imaging [26]; to increase the robustness of these measurements, data filtering or gamma-variate fitting has been proposed, which considerably complicates the post-processing. In contrast, the time-domain wavelet transform is inherently robust in the presence of noise and can be applied without prior optimization of noise-reducing filtering or fitting procedures.

In direct comparison, the wavelet-derived parameters provide an at least equal performance as the conventional attenuation-time-course parameters measured after gamma-variate fitting to improve the parameter robustness.

The maximum AUC obtained from the proposed wavelet parameters was slightly (although not statistically significantly) higher than the maximum AUC obtained from the conventional parameters.

The linear correlation coefficients between conventional and wavelet-based parameters

demonstrate high linear correlations for *A* as well as for *T*, which agrees with the fact that there is no significant improvement using our proposed parameters compared to the reference standard. However, the conventional and wavelet-based width parameters (*W*) correlate only weakly. This might be explained by greater instabilities and influence of noise in the determination of the (conventional) FWHM parameter.

A limitation of this study is the relatively small cohort size of 14 subjects, which, however, was sufficiently large to demonstrate the feasibility of the proposed technique and the statistically significant differences between evaluations with a single parameter and with FLDA-combined parameters. A second limitation is the missing clinical evaluation of the proposed method in patients with pathologies, which was beyond the scope of this feasibility study. In particular, diseased arterial vessels present in patients with pathologies may exhibit e. g. delayed arterial enhancement, which could complicate the vessel classification. Future studies in larger patient groups with different pathologies are required to evaluate the classification performance under these conditions. Another limitation is the restriction on a single wavelet (the Paul wavelet of order 1) as mother wavelet of the transform. The wavelet analysis can be performed with about any function that acts as band-pass and whose mean is zero; therefore, the selection of the optimal mother wavelet is essential for the entire analysis. Although very good classification results could be obtained using the Paul wavelet, further systematic investigations with a multitude of wavelet families are necessary and will be performed in a future study. Another possible application to be assessed in future studies is the ability of the proposed wavelet approach to support the characterization of brain parenchyma similar to conventional CT perfusion post-processing.

In conclusion, a new method to classify arterial and venous vessels with high accuracy was introduced based on the time-domain wavelet transform of dynamic CT perfusion data in combination with linear (Fisher's linear discriminant analysis) or non-linear (logistic regression or support vector machine) multidimensional classification techniques.

References

1 J. Beier, T. Büge, C. Stroszczynski, H. Oellinger, E. Fleck, and R. Felix, "2D- und 3D-parameterbilder zur analyse der kontrast-mittelverteilung bei dynamischen CT- und MR-untersuchungen.," Radiologe 38, 832–840 (1998).

2 E.J. Smit, E. -j. Vonken, I.C. van der Schaaf, A.M. Mendrik, J.W. Dankbaar, A.D. Horsch, T. van Seeters, B. van Ginneken, and M. Prokop, "Timing-Invariant Reconstruction for Deriving High-Quality CT Angiographic Data from Cerebral CT Perfusion Data.," Radiology 263, 216–225 (2012).

3 L. Havla, K.M. Thierfelder, S.E. Beyer, W.H. Sommer, and O. Dietrich, "Wavelet-based calculation of cerebral angiographic data from time-resolved CT perfusion acquisitions," Eur. Radiol. 25(8), 2354–2361 (2015).

4 S.J. Riederer, C.R. Haider, and E.A. Borisch, "Time-of-arrival mapping at three-dimensional time-resolved contrast-enhanced MR angiography.," Radiology 253(2), 532–42 (2009).

5 T. Struffert, S. Ott, M. Kowarschik, F. Bender, E. Adamek, T. Engelhorn, P. Gölitz, S. Lang, C.M. Strother, and A. Doerfler, "Measurement of quantifiable parameters by time-density curves in the elastase-induced aneurysm model: first results in the comparison of a flow diverter and a conventional aneurysm stent.," Eur. Radiol. 23(2), 521–7 (2013).

6 J.J. Barfett, J. Fierstra, P.W.A. Willems, D.J. Mikulis, and T. Krings, "Intravascular functional maps of common neurovascular lesions derived from volumetric 4D CT data.," Invest. Radiol. 45(7), 370–7 (2010).

7 L. Havla, M. Schneider, K.M. Thierfelder, S.E. Beyer, B. Ertl-Wagner, W.H. Sommer, and O. Dietrich, "Validation of a method to differentiate arterial and venous vessels in CT perfusion data using linear combinations of quantitative time-density curve characteristics.," Eur. Radiol. 25(10), 2937–44 (2015).

8 K.M. Thierfelder, L. Havla, S.E. Beyer, B. Ertl-Wagner, F.G. Meinel, L. von Baumgarten, H. Janssen, H. Ditt, M.F. Reiser, and W.H. Sommer, "Color-coded cerebral computed tomographic angiography: implementation of a convolution-based algorithm and first clinical evaluation in patients with acute ischemic stroke.," Invest. Radiol. 50(5), 361–5 (2015).

9 D.L. Donoho and J.M. Johnstone, "Ideal spatial adaptation by wavelet shrinkage," Biometrika 81(3), 425–455 (1994).

10 M. Farge, "Wavelet Transforms And Their Applications To Turbulence.," Annu. Rev. Fluid Mech. 24, 395–457 (1992).

11 C. Torrence and G.P. Compo, "A Practical Guide to Wavelet Analysis.," Bull. Am. Meteorol. Soc. 79, 61–78 (1998).

12 S. Sourbron, A.F. Biffar, M. Ingrisch, Y. Fierens, and R. Luypaert, "PMI0.4: platform for research in medical imaging.," in Proc. ESMRMB, Antalya(2009).

13 S. Klein, M. Staring, K. Murphy, M.A. Viergever, and J.P.W. Pluim, "elastix: a toolbox for intensity-based medical image registration.," IEEE Trans. Med. Imaging 29(1), 196–205 (2010).

14 R.A. Fisher, "The use of multiple measurements in taxonomic problems.," Ann. Eugen. 7, 179–188 (1936).

15 M.J. Schneider, C.C. Cyran, K. Nikolaou, H. Hirner, M.F. Reiser, and O. Dietrich, "Monitoring Early Response to Anti-Angiogenic Therapy: Diffusion-Weighted Magnetic Resonance Imaging and Volume Measurements in Colon Carcinoma Xenografts.," PLoS One (2014).

16 R.C. Gentleman et al., "Bioconductor: open software development for computational biology and bioinformatics.," Genome Biol. 5(10), R80 (2004).

17 M. Slawski, A.-L. Boulesteix, and C. Bernau, CMA: Synthesis of microarray-based classification, (2009).

18 C. Cortes and V. Vapnik, "Support-Vector Networks," Mach. Learn. 20(3), 273–297 (1995).

19 A. Karatzoglou, A. Smola, K. Hornik, and A. Zeileis, "kernlab - - An S4 Package for Kernel Methods in R," J. Stat. Softw. 11(9), 1–20 (2004).

20 M. Kuhn, "Caret: Classification and regression training," R package, 2015.

21 W. J.Youden, "Index for rating diagnostic tests," Cancer 3(1), 32–35 (1950).

22 X. Robin, N. Turck, A. Hainard, N. Tiberti, F. Lisacek, J.-C. Sanchez, and M. Müller, "pROC: an open-source package for R and S+ to analyze and compare ROC curves.," BMC Bioinformatics 12, 77 (2011).

23 E.R. DeLong, D.M. DeLong, and D.L. Clarke-Pearson, "Comparing the areas under two or more correlated receiver operating characteristic curves: a nonparametric approach.," Biometrics 44, 837–845 (1988).

24 C. Bonferroni, "Teoria statistica delle classi e calcolo delle probabilita," Pubbl. del R Ist. Super. di Sci. Econ. e Commer. di Firenze 8, 3–62 (1936).

25 R. Kohavi, "A Study of Cross-Validation and Bootstrap for Accuracy Estimation and Model Selection," in Int. Jt. Conf. Artif. Intell.(1995), pp. 1137–1143.

26 Y. Chen, L. Shi, Q. Feng, J. Yang, H. Shu, L. Luo, J. Coatrieux, and W. Chen, "Artifact Suppressed Dictionary Learning for Low-dose CT Image Processing," Med. Imaging, IEEE Trans. PP(99), 1 (2014).